Force Profiles of a Linear Switched Reluctance Motor Having Special Pole Face Shapes

N.C.LENIN[1], R.ARUMUGAM[2], V. CHADRESEKAR[3]
[1]*St.Joseph's College of Engineering, Chennai, 600 119, India*
[2]*SSN College of Engineering, Chennai, India*
[2]*Arunai College of Engineering, Thiruvannamalai, India*
nclenin@gmail.com

***Abstract*—In this paper, the results of a finite element analysis are carried out on an new stator geometry of a three phase longitudinal flux Linear Switched Reluctance Motor (LSRM). In the new geometry, pole shoes are affixed to the stator poles. Static and dynamic characteristics for the proposed structure have been highlighted. Motor performance for variable load conditions is discussed. Frequency spectrum analyses of force profile using the fast Fourier transform (FFT) are described to predict the vibration frequencies. The 2-Dimensional (2-D) finite element analysis (FEA) and the experimental results of this paper prove that LSRMs are one of the strong candidates for linear propulsion drives.**

***Index Terms*—Linear switched reluctance motor, finite element analysis, force ripple, FFT**

NOMENCLATURE

w_{sp}	width of the stator pole	(m)
w_{ss}	width of the stator slot	(m)
w_{sy}	stator back iron thickness	(m)
h_{sp}	stator pole height	(m)
w_{tp}	width of the translator pole	(m)
w_{ts}	width of the translator slot	(m)
w_{ty}	translator back iron thickness	(m)
h_{tp}	translator pole height	(m)
l_g	air gap length	(m)
V_{rated}	rated voltage	(V)
I_{rated}	rated current	(A)
V	velocity	(m/s)
F_{max}	maximum force	(N)
F_{min}	minimum force	(N)
F_{avg}	average force	(N)
F_L	load force	(N)
P_m	mechanical power output	(W)
N_{ph}	No. of turns per phase	
L_{stack}	stack length	(m)
L_{min}	minimum inductance	(H)
L_{max}	maximum inductance	(H)
x*	position	(m)
$\dot{x}$*	commanded velocity	(m/s)
$\dot{x}$	actual velocity	(m/s)
F_e*	commanded force	(N)
F_e	actual force	(N)
k	phase a, b, c.	
f_k	force distribution function	
F_k*	distributed commanded force	(N)
F_{k+n}*	distributed commanded force for N no. phases	(N)
I_k*	current command	(A)
I_k	actual current	(A)
V_k*	reference phase voltage	(V)
V_k	instantaneous phase voltage	(V)
L_k	phase inductance	(H)
x	displacement in propulsion force direction	(m)
g_k	rate of change of inductance with respect to x direction	(N/A^2)

I. INTRODUCTION

Linear switched reluctance motors are an attractive alternative to linear induction or synchronous machines due to lack of windings on the stator or translator structure, easier manufacturing and maintenance, good fault tolerance capability [1]. LSRMs are classified as (a) longitudinal flux (b) transverse flux. This paper is dedicated to the longitudinal flux LSRM. A design procedure for longitudinal-flux LSRM has been described in [2]. Other types of longitudinal-flux LSRMs are presented in [3], with coupled flux paths, and in [4] with uncoupled flux paths for a magnetic levitation system. A high force longitudinal-flux double-sided double-translator LSRM has been analyzed in [5]. Longitudinal-flux LSRMs have been proposed for applications such as precise motion control [6], [7] and as propulsion systems for railway vehicles [8] or vertical elevators [9]–[11]. Recently, a detailed sensitivity analysis of double sided LSRM parameters based on [12] has been presented in [13].

In despite of the various advantages, LSRMs has some drawbacks such as high force ripple, vibration, acoustic noise and need of power electronic converters. Several efforts to reduce or eliminate the torque ripple of the rotary switched reluctance motors (RSRMs) have been presented in the literature [14-18]. Multi phase excitation to reduce the force ripple in the LSRM has been explained in [19]. However, the previous method considerably increases the copper losses. In this paper a novel stator structure for a longitudinal flux LSRM is proposed to reduce the force ripple. Two dimensional (2D) finite element analysis (FEA) is carried out to predict the performance of the conventional and the proposed structures.

A control strategy for the proposed LSRM is dynamically simulated, which consists of force and velocity control loops. A trapezoidal velocity profile is used to control travel position smoothly during acceleration, deceleration, and stop of the motor. Conventional proportional–integral controller is used for the current and velocity control loops [10]. Further, the influence of load variation on some of the parameters like the velocity, current, and the efficiency of the motor are studied

When the frequency of the exciting force is close or equal to any of the natural frequencies of the machine, then

Digital Object Identifier 10.4316/AECE.2010.04021

resonance occurs, which results in dangerous deformations and vibrations and a substantial increase in noise [20]. FFT steps to analyze ripple in the force profile of the LSRM is presented.

The organization of the paper is as follows: Section II presents new stator geometry for LSRMs that improves the force profile and FEA results for the conventional and the proposed structures. Section III contains dynamic simulation results of the proposed structure. Frequency spectrum analysis of the force profile using the FFT is highlighted in section IV. Experimental results from the prototype machine and their correlation with FEA results are presented in Section V. Conclusions and future work are summarized in Section VI.

II. Force Ripple Analysis Using an Alternative Geometry

A. Definition, Sources of the force ripple and techniques to reduce it

Assuming that the maximum value of the static force as F_{max}, the minimum value that occurs at the intersection point of two consecutive phases as F_{min}, and the average force as F_{avg}, the percentage force ripple may be defined as (1)

$$\%Force\ Ripple = \frac{F_{max} - F_{min}}{F_{avg}} \times 100 \qquad (1)$$

The causes of the force ripple in LSRMs are mainly due to the switching of phase currents into its windings and the highly nonlinear nature of the phase inductance variation when the translator moves. These force pulsations contribute to vibrations and acoustic noise in LSRMs.There are two approaches to force profile improvement. One approach is to suitably shape the input excitation current profile by using an electronic control of the power controllers. The second approach is to modify the geometry of the poles of the stator and translator. This research makes an attempt to examine the force profile by the geometry modifications approach, by providing pole shoes on the stator poles.

B. Effect of stator pole shaping on the force profile

This sensitivity study aims mainly to determine the improvement in the force profile when the stator pole width gets varied. The conventional LSRM which is considered in this paper is shown in fig.1. The specifications of the conventional machine are given in Table 1.

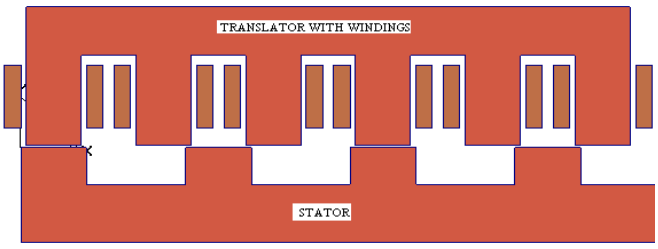

Figure. 1. 2D cross sectional view of the conventional LSRM

Table 1
Specifications and Dimensions of the Studied LSRM

l_g = 1.5 mm	w_{sp} = 21 mm
F_{max} = 120 N	h_{sp} = 30 mm
L_{stack} = 40 mm	w_{sy} = 35mm
Steel type (Stator) - M 45	w_{ss} = 31 mm
Steel type (Translator) - M 45	w_{ts} = 26 mm
Travel length= 2 m	h_{tp} = 48 mm
V_{rated} = 120 V	w_{tp} = 13 mm
I_{rated} = 10 A	w_{ty} = 30mm
N_{ph} = 396	Wire size = AWG 18

The width of the stator pole is varied from 16mm to 21mm in steps. The translator geometry remains unchanged throughout the sensitivity study. The height of the stator pole is fixed. The field analysis has been carried out for a phase excitation of 10 A. The predicted propulsion force, normal force,inductances and average force profiles are shown in fig.2. Table 2 summarizes the comparison of the studied configurations.

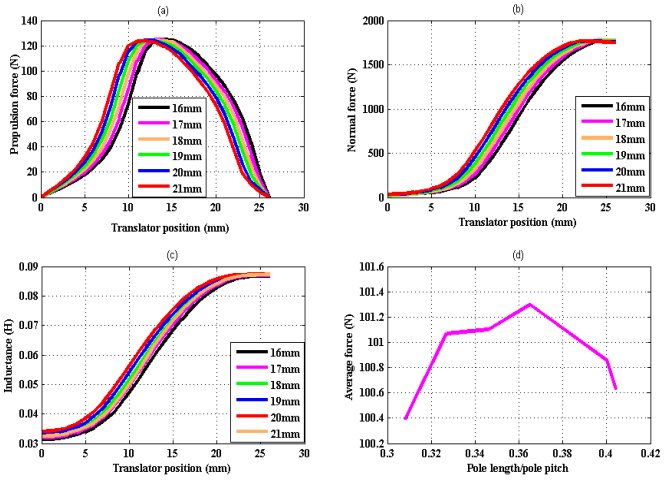

Figure. 2. Force and Inductance for various stator pole widths (without pole shoes)

From the Table 2 it can be observed that, when the stator pole width is increased, there is a reduction in the average force, which is not large after a certain point. Fig.2(d) shows the stator pole length/pole pitch vs. average force. From fig.2(d), we inferred that, the maximum average force and low force ripple occurs, when the pole width is 19mm.

Table 2
Comparison of Force Ripple for Various Stator Pole Widths (without pole shoes)

W_{sp} (mm)	F_{min} (N)	F_{max} (N)	F_{avg} (N)	% ripple	L_{min} (H)	L_{max}(H)
16	67.33	124.87	100.39	60.38	0.02972	0.08626
17	67.91	124.70	101.07	57.68	0.03019	0.08658
18	68.23	124.57	101.10	55.88	0.03071	0.08683
19	68.32	124.11	101.30	53.41	0.03125	0.087
20	68.28	124.34	100.86	56.16	0.03184	0.08713
21	67.88	123.90	100.63	55.67	0.03246	0.08725

C. Force Ripple Minimization Using Stator Pole Shoes

In this section, improving the force profile using stator pole shoes is investigated by 2-D finite-element analysis. The difference between the conventional and the proposed stator poles are shown in fig.3. The cross sectional view of the proposed LSRM is shown in fig.4.

Figure .3. (a) Conventional (b) Proposed

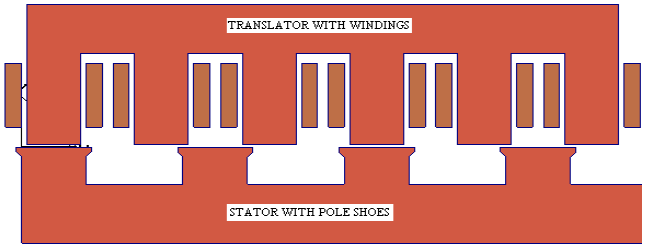

Figure. 4. 2D cross sectional view of the proposed LSRM

The aim in proposing the stator pole shoe is to widen the stator pole width to smoothen the force profile. The analysis is carried out on the conventional LSRM with a pole shoe, which is affixed on the stator poles. The width of the stator pole shoe is 4mm. The stator pole width is varied from 16mm to 20mm in steps. The width of the pole shoe and overall height of the stator pole are maintained constant. The mutual inductance and leakage effects are neglected. The simulation is presented for an excitation current of 10 A. The predicted propulsion force, normal force and inductance profiles are shown in fig.5.

Table 3 summarizes the comparisons of the studied configurations with pole shoes. Fig.5(d) shows the stator pole length/pole pitch vs. average force. From fig.5(d), the maximum average force and low force ripple occurs, when the stator pole width is 19mm with a 4mm pole shoe.

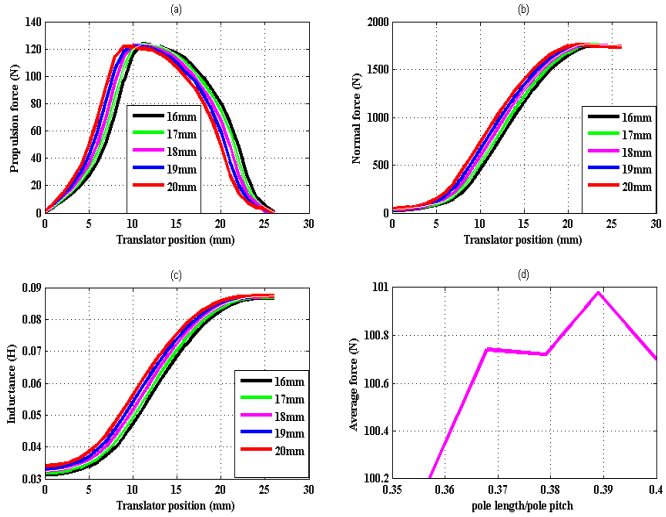

Figure. 5. Force and Inductance for various stator pole widths (with pole shoes)

TABLE 3
COMPARISON OF FORCE RIPPLE FOR VARIOUS STATOR POLE WIDTHS (WITH POLE SHOES)

W_{sp} (mm)	F_{min} (N)	F_{max} (N)	F_{avg} (N)	% ripple	L_{min} (H)	L_{max}(H)
16	69.30	123.33	100.2	53.97	0.03130	0.08681
17	68.83	122.76	100.74	53.54	0.03194	0.08708
18	68.84	122.18	100.72	52.95	0.03260	0.08723
19	68.62	121.78	100.98	52.64	0.03327	0.08730
20	68.27	121.77	100.70	53.12	0.03403	0.08737

D. Discussion on 2-D FEA Results

This section addresses an important technical problem in LSRMs, specifically the force ripple. A study of the same by modifying the stator pole and affixing stator pole shoes and the observations made from the 2-D FEA used for field simulation results on this geometry are reported. The provision of stator pole shoes improves the force profile and reduces the force ripple at the maximum force regions. Hence, the maximum force is allowed to remain the same for more positions of the translator. The extent of the low force region around the unaligned position is reduced due to the addition of pole shoes. From Table 3 it can be observed that, as the stator pole width is increased, keeping the stator pole shoe width as constant, there is a reduction in the average force, which is not large after certain a point. The sensitivity study also depicts that any reduction in the width of the stator pole for the same variations of the pole shoe arcs, contributes to a loss of the average force. It is generally accepted that decreasing the stator pole width will decrease the aligned inductance with negligible effect on the unaligned inductance. This is reflected in Table 2 obtained from a 2-D FEA field simulation. Finally, the stator volume, stator mass and the %force ripple reduction are compared in Table 4. From the Table 4 we infered that, the proposed LSRM (19mm stator pole width) has high force density, less force ripple, less volume and mass when compared to the conventional machine. So, for the other analysis in this paper we prefer LSRM with pole shoe having 19mm pole width.

TABLE 4
COMPARISON OF VOLUME, MASS AND FORCE RIPPLE

W_{sp} (mm)	Volume (m^3)		Mass (kg)		Force ripple reduction (%)
	Without pole shoes	With pole shoes	Without pole shoes	With pole shoes	
16	0.00243	0.00238	18.68	18.37	10.62
17	0.00245	0.00242	18.88	18.64	7.18
18	0.00247	0.00245	19.1	18.92	5.24
19	0.0025	0.00249	19.28	19.19	1.44
20	0.00253	0.00252	19.48	19.46	5.41
21	0.00255	NA	19.67	NA	NA

NA: not analyzed in this paper.

III. DYNAMIC SIMULATION

A. Force and Velocity Control

For a vertical or horizontal applications, the LSRMs needs a precise control strategy consisting of force, current, velocity, and position controls, as shown in fig.6. Force control with a force distribution function (FDF) is used to control the LSRM. A trapezoidal velocity profile is used to obtain the desired response curve of the position. In addition, current and velocity controls with proportional–integral (PI) control for the proposed LSRM are explained in this section. The proposed LSRM is simulated at 0.15 m/s velocity. The data for the dynamic simulation is obtained from the FEA, which is shown in fig.5. The remaining motor parameters and input specifications are summarized in the Table 1.

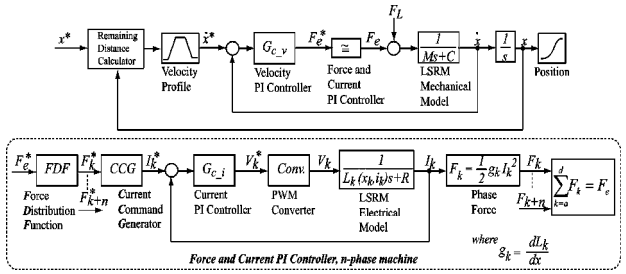

Figure. 6. Control block diagram for the proposed LSRM

During starting, the deceleration command is given at 0.5 m, and during stopping, the deceleration command is given at 0.1 m. The duration for holding at the stop position is set to 1sec. Fig.7 shows the simulation results of the position, velocity, phase current, and generated force of the LSRM at 0.15 m/s.

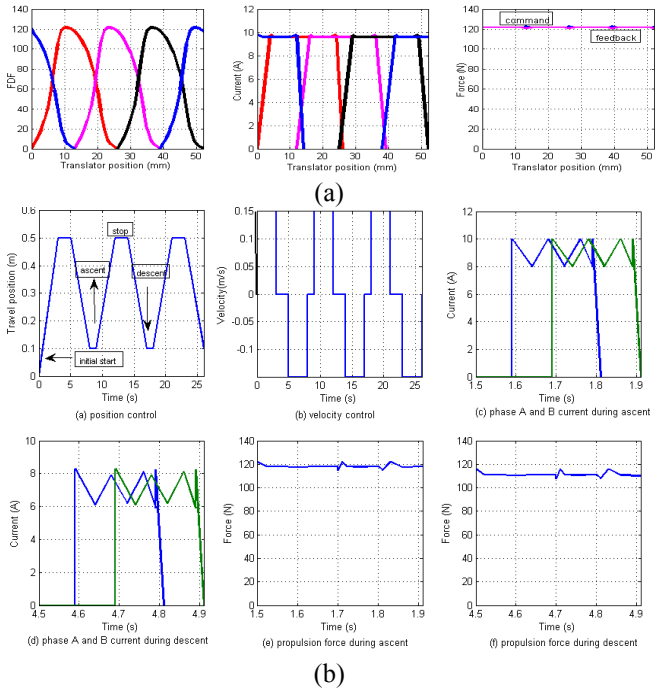

Figure. 7. Dynamic analysis (a) Force control (b) Velocity control

In fig.7 (a) the designed LSRM successfully carries the load at 0.15 m/s producing an excellent velocity and position control performance. After the deceleration command is given at 0.5 m and 0.1 m during starting and stopping respectively, the motor stops at 0.49 m and 0.1 m, where the velocity command from the velocity profile is zero. Under continuous operation, the current amplitude values in starting and stopping are 9.6 and 8.4 A/phase, respectively. In addition, the average force produced is 1191.7 N during acceleration and 113.6 N during deceleration.

B. Motor Performance for Variable Load Conditions

In practice, motors operate with changing load conditions. The influence of load variation on some of the parameters like the velocity, current, and the efficiency of the motor are studied. The results shown in Table 5 are obtained when the circuit is turned ON at the point when the inductance starts to increase and turned OFF before it starts to decrease.

TABLE 5
INFLUENCE OF LOAD ON MOTOR PERFORMANCE

F_L (N)	I (A)	V (m/s)	Input power (W)	Output power (W)	Efficiency (%)
2	2.09	10.42	57.85	26.12	45.15
5	3.28	8.03	65.84	31.46	47.78
10	4.72	6.40	91.39	39	42.67
20	5.31	4.02	114.61	46.99	41
40	6.19	3.35	151.36	57.70	38.12
60	7.87	2.65	181.32	63.66	35.11
80	8.29	1.28	196.36	67	34.12
100	9.79	0.5	214.45	71.11	33.16
120	10.5	0.15	255.84	77.8	30.41

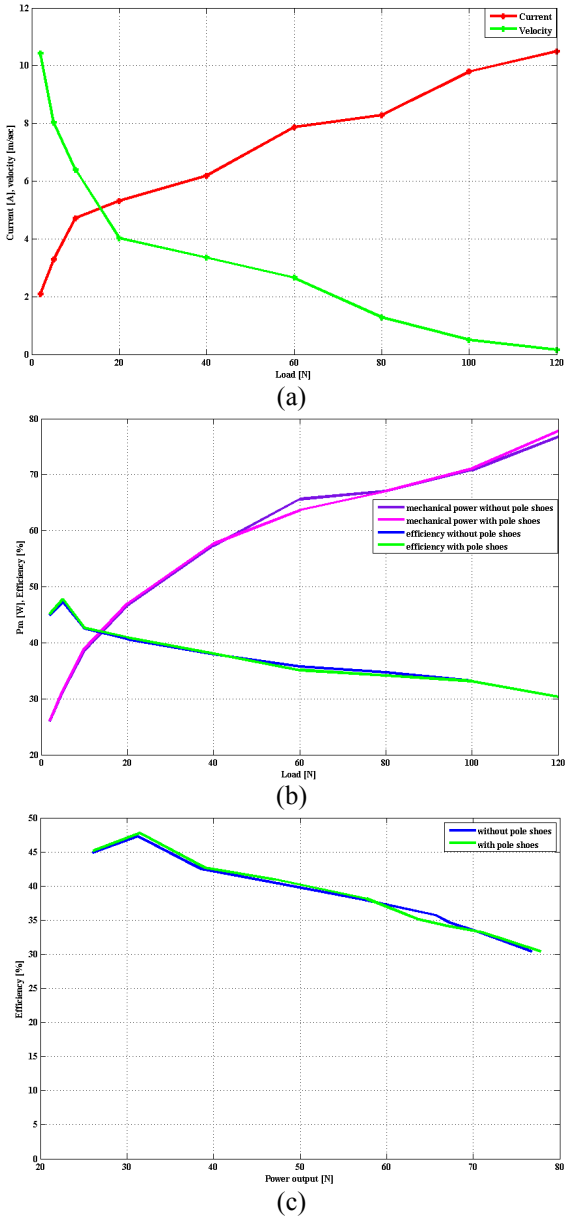

Figure. 8. (a) Variation of current and velocity with load (b) Variation of P_m, efficiency with load (c) Variation of efficiency with P_m

Fig.8 (a) shows the velocity and current variation for different load conditions. The velocity steadily decreases with an increase in load. This characteristic reminds of the speed-load characteristic of a series DC motor. Fig.8 (b) shows the characteristics of mechanical power P_m, and the efficiency with change in load. It can be seen that, initially as the load increases the efficiency increases and when load is further increased the efficiency started to decrease. Fig.8 (c) shows the characteristics of the efficiency with change in

mechanical power P_m. It can be seen that, the efficiency is high at most of the cases, encouraging the proposal of the pole shoe concept in LSRM.

IV. Fast Fourier Transform Application to LSRM

From the results of the 2-D finite-element field analysis performed earlier (fig.4 and fig.5), the force versus translator position will be known. A script (.m) file is written in a MATLAB environment which contains a sequence of instructions to store the array of the four phases. The FFT is applied to the net force profile after the elimination of the dc offset. Since the FFT transforms the available data in the time domain into the frequency domain, the available force versus translator position profile must be converted into the force versus time profile. In MATLAB, the command fft (x, p), where 'x' is the force array and 'p' is 512, denoting 512 point fft will be solved to produce a complex discrete Fourier transform (DFT) of force. The absolute value of the obtained complex DFT will form the magnitude axis. The magnitude plot is obtained by plotting the magnitude versus frequency. Note that the FFT is performed on stator with out pole shoes and stator with pole shoes which is having 19mm stator pole width.

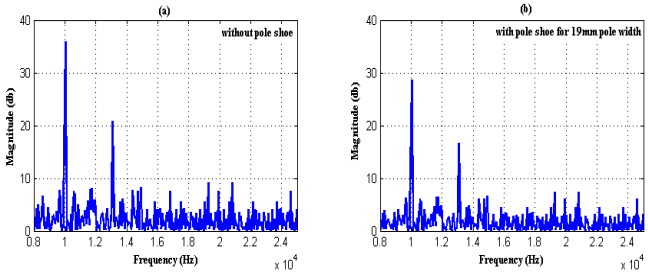

Figure. 9. FFT output (a) without pole shoe (b) with pole shoe

Fig.9 shows the results of the frequency spectrum analysis for the case of stator with and wuthout pole shoes. The frequency corresponding to these decibel (dB) peaks can be identified from the plot. Table 6 and Table 7 shows the dominant frequencies in hertz and its amplitude in dB for the conventional and the proposed structures respectively. It is observed that the dB peaks occurs at a certain same frequencies as before (without pole shoes) but the magnitude of the dB peaks is reduced by considerable margin, encouraging the proposal of stator pole shoes.

TABLE 6
DOMINANT RIPPLE FREQUENCIES AND ITS AMPLITUDE FOR STATOR WITHOUT POLE SHOES

Predominant ripple frequencies (Hz)	Amplitude (dB)
10,050	35.85
13,100	20.8
14,910	8.29
19,260	9.185

TABLE 7
DOMINANT RIPPLE FREQUENCIES AND ITS AMPLITUDE FOR STATOR WITH POLE SHOES

Predominant ripple frequencies (Hz)	Amplitude (dB)
10,050	28.68
14,620	16.64
19,260	7.348
22,420	7.21

V. Experimental Results

Fig.10 shows the actual experimental setup for the prototype LSRM with the stator pole shoe that is used as a material carrying vehicle in the laboratory. The experimental road is 2 m long and translator weight is 12 kg. It should be noted that the present setup is intended for development purposes only.

(a) (b) (c)

Figure.10 Experimental setup of (a) LSRM and converter (b) Driver circuit (c) PC along with measuring instruments

The inductance for the different positions at rated current is measured by locking the translator at each position. A constant current is applied to a phase and is turned off and the falling current profile is computed. The time constant is measured from the profile and hence the inductance is calculated. The measured values of inductance are plotted alongside the FEA results in fig.11. A comparison of inductance values at aligned and unaligned positions are given in Table 8 at the rated current. Fig.12 shows actual phase voltage and phase current waveforms of the LSRM.

TABLE 8
COMPARISON OF THE CALCULATED AND THE MEASURED INDUCTANCE AT RATED CURRENT

Method	Inductance (H)	
	Aligned	Unaligned
FEA	0.0873	0.0332
Measured	0.0884	0.0321

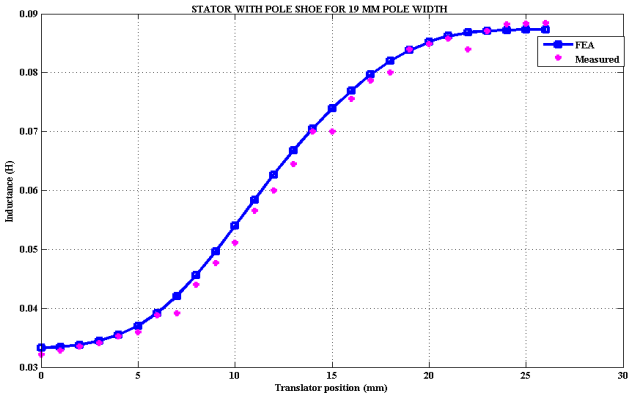

Figure.11. comparison of FEA and measured inductance values at rated current

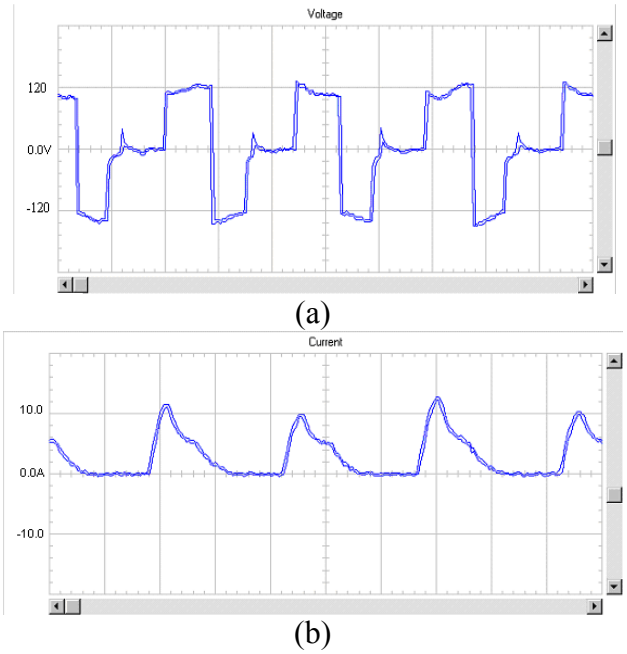

Figure.12. Experimental waveforms during single pulse operation (a) Actual phase voltage of LSRM (b) Actual phase current of LSRM

I. CONCLUSION

A modification of the stator geometry by the provision of stator pole shoes has been presented. A prototype LSRMs is modeled, simulated, analyzed, developed, and experimentally validated with the conventional control strategy. The proposed structure reduces the force ripple by 5.44%, volume by 2.35% and mass by 2.44% compared to the conventional machine. Force density is high in the proposed structure. Furthermore, the maximum efficiency occures at a load force of 5 N, which is also high when compared to the conventional LSRM. The FFT method to analyze the ripple in the force profile of the LSRM are presented. This methodology is comparatively simpler than the most widely used finite-element vibration analysis procedure for mode frequency identification. There is a good agreement between measurement results and FEA values of the inductance profile. The proposed stator pole shoe geometry research can be further extended to study the thermal, stress and vibration analyses.

REFERENCES

[1] T. J. E. Miller. *Switched Reluctance Motor and Their Control.* Hillsboro, OH: Magna Phys., 1993.

[2] L. Byeong-Seok, B. Han-Kyung, V. Praveen, and R. Krishnan, "Design of a linear switched reluctance machine," *IEEE Trans. Ind. Appl.*, vol. 36,no. 6, pp. 1571–1580, Nov./Dec. 2000.

[3] N. Chayopitak and D. G. Taylor, "Design of linear variable reluctance motor using computer-aided design assistant," in *Proc. IEEE Int. Conf. Elect. Mach. Drives*, May 2005, pp. 1569–1575.

[4] Z. Sun, N. C. Cheung, J. Pan, S. W. Zhao, and W.-C. Gan, "Design and simulation of a magnetic levitated switched reluctance linear actuator system for high precision application," in *Proc. IEEE ISIE*, Jun. 30–Jul. 2, 2008, pp. 624–629.

[5] U. S. Deshpande, J. J. Cathey, and E. Richter, "High-force density linear switched reluctance machine," *IEEE Trans. Ind. Appl.*, vol. 31, no. 2, pp. 345–352, Mar./Apr. 1995.

[6] J. Pan, N. C. Cheung, and J. Yang, "High-precision position control of a novel planar switched reluctance motor," *IEEE Trans. Ind. Electron.*, vol. 52, no. 6, pp. 1644–1652, Dec. 2005.

[7] S. W. Zhao, N. C. Cheung, W.-C. Gan, J. M. Yang, and J. F. Pan, "A self-tuning regulator for the high-precision position control of a linear switched reluctance motor," *IEEE Trans. Ind. Electron.*, vol. 54, no. 5, pp. 2425–2434, Oct. 2007.

[8] L. Kolomeitsev, D. Kraynov, F. Pakhomin, F. Rednov, E. Kallenbach, V. Kireev, T. Schneider, and J. Böcker, "Linear switched reluctance motor as high efficiency propulsion system for railway vehicles," in *Proc. SPEEDAM*, 2008, pp. 155–160.

[9] H. S. Lim and R. Krishnan, "Ropeless elevator with linear switched reluctance motor drive actuation systems," *IEEE Trans. Ind. Electron.*, vol. 54, no. 4, pp. 2209–2218, Aug. 2007.

[10] H. S. Lim, R. Krishnan, and N. S. Lobo, "Design and control of a linear propulsion system for an elevator using linear switched reluctance motor drives," *IEEE Trans. Ind. Electron.*, vol. 55, no. 2, pp. 534–542, Feb. 2008.

[11] N. S. Lobo, H. S. Lim, and R. Krishnan, "Comparison of linear switched reluctance machines for vertical propulsion application: Analysis, design, and experimental correlation," *IEEE Trans. Ind. Appl.*, vol. 44, no. 4,pp. 1134–1142, Jul./Aug. 2008.

[12] R. Arumugam, J. F. Lindsay, and R. Krishnan, "Sensitivity of pole arc/pole pitch ratio on switched reluctance motor performance," in *Conf. Rec.IEEE IAS Annu. Meeting*, Pittsburgh, PA, Oct. 1988, vol. 1, pp. 50–54.

[13] J. G. Amoros, and P. Andrada, "Sensitivity Analysis of Geometrical Parameters on a Double-Sided Linear Switched Reluctance Motor," *IEEE Transactions on Industrial Electronics*, vol. 57, no. 1, pp. 311-319, Jan. 2010.

[14] D. Schramm, B. W. Williams, and T. C. Green, "Torque ripple reduction of switched reluctance motors by phase current optimal profiling," *Proc. IEEE PESC'92*, 1992, pp. 857–860.

[15] M. Moallem, C. M. Ong and L. E. Unnewehr, "Effect of rotor profiles on the torque of a switched reluctance motor," *IEEE Trans. on Ind. Applicat.*, vol. 28, no. 2, pp. 364-369, Mar./Apr. 1992.

[16] Iqbal Hussain and M. Ehsani, "Torque Ripple Minimization in Switched Reluctance Motor Drives by PWM Current Control", *IEEE Trans., on Power Electronics*, vol.11, No.1, January 1996, pp: 83-88.

[17] R. Rabinovici, "Torque ripple, vibrations, and acoustic noise in switched reluctance motors", *HAIT Journal of Science and Engineering B*, vol. 2, Issues 5-6, pp. 776-786, July 2005.

[18] C.Neagoe, A.Foggia and R.Krishnan, "Impact of pole tapering on the electromagnetic force of the switched reluctance motor," *in Conf. Rec. IEEE Electric Machines and Drives Conference*, 1997, pp. WA1/2.1- WA1/2.3.

[19] Han-Kyung Bae, B. S. Lee, Praveen Vijayaraghavan, R. Krishnan, "A linear switched reluctance motor: Converter and Control," *IEEE Transactions on Industry Applications*, vol.36, no.5, Sep/Oct 2000.

[20] Derrick. E. Cameron, Jeffrey. H. Lang and Stephen. D. Umans, "The origin and reduction of acoustic noise in doubly salient variable-reluctance motors," *IEEE Transactions on Industry Applications*, vol.28, No.6, Nov. /Dec. 1992.